J Mol Model (2016) 22: 121
DOI 10.1007/s00894-016-2976-2

ORIGINAL PAPER

Does the position of the electron-donating nitrogen atom in the ring system influence the efficiency of a dye-sensitized solar cell? A computational study

Abul Kalam Biswas[1,4] · **Sunirmal Barik**[1] · **Amitava Das**[2,3] · **Bishwajit Ganguly**[1,4]

Received: 12 May 2015 / Accepted: 5 April 2016 / Published online: 7 May 2016

Abstract We have reported a number of new metal-free organic dyes (**2–6**) that have cyclic asymmetric benzotripyrrole derivatives as donor groups with peripheral nitrogen atoms in the ring, fluorine and thiophene groups as π-spacers, and a cyanoacrylic acid acceptor group. Density functional theory (DFT) and time-dependent DFT (TD-DFT) calculations were employed to examine the influence of the position of the donor nitrogen atom and π-conjugation on solar cell performance. The calculated electron-injection driving force (ΔG_{inject}), electron-regeneration driving force (ΔG_{regen}), light-harvesting efficiency (LHE), dipole moment (μ_{normal}), and number of electrons transferred (Δq) indicate that dyes **3**, **4**, and **6** have significantly higher efficiencies than reference dye **1**, which exhibits high efficiency. We also extended our comparison to some other reported dyes, **7–9**, which have a donor nitrogen atom in the middle of the ring system. The computed results suggest that dye **6** possesses a higher incident photon to current conversion efficiency (IPCE) than reported dyes **7–9**. Thus, the use of donor groups with peripheral nitrogen atoms appears to lead to more efficient dyes than those in which the nitrogen atom is present in the middle of the donor ring system.

Keywords DFT · TD-DFT · Dye-sensitized solar cells · Organic dyes · Position effect

Electronic supplementary material The online version of this article (doi:10.1007/s00894-016-2976-2) contains supplementary material, which is available to authorized users.

✉ Amitava Das
a.das@ncl.res.in

✉ Bishwajit Ganguly
ganguly@csmcri.org

[1] Computation and Simulation Unit (Analytical Discipline and Centralized Instrument Facility), CSIR—Central Salt and Marine Chemicals Research Institute, Bhavnagar 364002, India

[2] Organic Chemistry Division, CSIR—National Chemical Laboratory, Pune 411008, India

[3] CSIR—National Chemical Laboratory, Academy of Scientific and Innovative Research, Pune 411008, India

[4] CSIR—Central Salt and Marine Chemicals Research Institute, Academy of Scientific and Innovative Research, Bhavnagar, Gujarat 364002, India

Introduction

Dye-sensitized solar cells (DSSCs) have been actively pursued in the search for new renewable energy sources, as they have many advantages over silicon-based solar cells, including low cost, easy production, and flexibility [1–9]. DSSCs have been extensively studied since O'Regan and Grätzel published their seminal work in 1991 [10]. These devices are generally composed of organic or inorganic dyes adsorbed on an inorganic n-type semiconductor, a platinized counter electrode, and a redox electrolyte [11]. The highest power conversion efficiencies (PCEs) of DSSC devices have been achieved by using metal-based dyes [12–24]. Among various DSSCs, those derived from ruthenium(II)–polypyridyl complexes have shown the best photostability as well as photocurrent conversion efficiencies [25]. Such dyes possess the highest PCEs because of their photochemical and electrochemical properties. However, it can be difficult to synthesize and purify the preferred Ru(II)–polypyridyl complexes [26]. Dyes based on heavy-metal ions are not environmentally friendly, and sources of ruthenium are limited [27]. Thus, metal-free sensitizers such as organic dyes have been studied and explored with a view to developing a new class of sensitizer dye molecules [13, 28–31]. In some cases, the utilization

of organic dye molecules as efficient DSSCs is hindered by their low stability, difficult syntheses, and the formation of aggregates on the semiconductor surface [13, 32]. However, efforts have been made to synthesize efficient organic dye molecules in order to achieve higher DSSC performance [13, 32]. Metal-free organic dyes have a D–π–A dipolar architecture, where a π-electron-rich moiety (D) is linked to a π-electron-poor end group (A) through a π-spacer. The choice of anchoring group also plays a crucial role in the efficiency of the DSSC [33]. Recent reports have revealed that modifying metal-free organic dyes structurally as well as electronically can significantly improve their absorption and overall efficiency, making them more useful for application in DSSCs [26].

A solar energy to electricity conversion efficiency of 6.8 % was achieved using an organic dye containing diarylamine as the donor unit, fluorene and thiophene as π-spacers, and cyanoacrylic acid as the anchoring group [34]. The performance of a DSSC is dependent on several different parameters, so the development of an efficient dye is a considerable challenge to both experimental and theoretical chemists [33].

DFT methods have been used to calculate the structural properties, electronic bands, optical excitation spectra, and charge-transport properties of organic/inorganic hybrid materials [35]. DFT and TDDFT methods have been found to be reliable tools for designing new dyes with appropriate optical, electrochemical, and physical properties for application in DSSCs [36]. Reports have suggested that CAM–B3LYP/6-31 + G* in combination with the conductor-like polarizable continuum model (CPCM) accurately reproduces the vertical transition energies of D–π–A organic dyes [37–39]. The nature of the anchoring group as well as the strength of coupling of the dye molecule to the semiconductor surface significantly influence the efficiency of the DSSC. Strong dye coupling reduces the possibility of desorption, enhances the cycle of use of the solar cell, and faciliates electron injection from the photoexcited singlet/triplet state(s) of the dye to the conduction band of the semiconductor. The electron injection rate is an important influence on the efficiency of a DSSC [40]. This injection rate can be calculated quantum chemically with reasonable accuracy by a range of methodologies [14, 36, 41–45]. Reports also suggest that the donor group of the dye molecule has a significant effect on solar cell performance. A wide variety of organic dyes containing various electron donors, such as dialkylamine groups [46, 47], coumarins [48–51], carbazole [52, 53], quinoxaline [54, 55], difluorenylphenylamine [56–62], julolidine [63], an electron-donating diphenyl amine moiety containing a methoxy group [64], di(*p*-tolyl)phenylamine [65], pyrrolidino, and ullazine [66], have been explored in DSSC design.

In the work reported in the present article, we performed a computational study to investigate the influence of cyclic asymmetric benzotripyrrole derivatives (**2**–**6**) as donor groups on DSSC efficiency. Phenyl-substituted derivatives of cyclic asymmetric benzotripyrrole can be prepared by the electropolymerization of indole-5-carboxylic acid and 5-cyanoindole [67] and the reaction of indole with nitrosobenzene in the presence of an acid [68]. Ruiz et al. have shown that asymmetric compounds present redshifted absorption and emission maxima compared to the corresponding symmetric compounds [69]. Asymmetric compounds also show improved fluorescence quantum yields [69]. The experimental results for organic dye **1** with diphenylamine as a donor group were found to be in good agreement with the corresponding computational results [34, 70, 71]. Therefore, in the present study, we used **1** as a reference dye to examine the efficiencies of a series of designed dyes (Fig. 1). The calculations were performed at the same level of theory as employed for **1**, and they predicted that the designed dyes **3**, **4**, and **6** possess higher efficiencies than reference dye **1** [70]. The designed dyes were compared with other recently reported donor systems that have a nitrogen atom in the middle of the ring system [66, 71, 72]. These comparisons highlighted the importance of the position of the nitrogen atom in the donor molecule.

Methods

Evaluation of key parameters

The energy conversion efficiency (η) of solar cell device can be determined using the following equation:

$$\eta = \mathrm{FF}\frac{V_{OC}J_{SC}}{P_{inc}}, \tag{1}$$

where V_{oc} is the open-circuit photovoltage, J_{sc} is the short-circuit current density, FF is the fill factor, and P_{inc} is the solar power incident on the cell.

The short-circuit current density, J_{sc}, in a DSSC is determined by the following equation [70]:

$$J_{sc} = \int_{\lambda}\mathrm{LHE}(\lambda)\Phi_{\mathrm{inject}}.\eta_{\mathrm{collect}}.\eta_{\mathrm{regen}}I_s(\lambda).\mathrm{d}\lambda, \tag{2}$$

where LHE(λ) is the light-harvesting efficiency at a given wavelength, calculated as LHE = 1 – 10^{-f}; f is the oscillator strength. Φ_{inject} is the electron-injection efficiency and η_{collect} denotes the charge-collection efficiency. Φ_{inject} is closely related to the driving force $\Delta G_{\mathrm{inject}}$ (for the injection of electrons from the excited states of dye molecules to the semiconductor substrate), which is calculated as the difference between the oxidation potential of the excited dye ($E^{\mathrm{dye}*}$) and the reduction potential of the CB of TiO_2 (E_{CB}, −4.00 eV) [73]:

$$\Delta G_{\mathrm{inject}} = E^{\mathrm{dye}*} - E_{\mathrm{CB}}. \tag{3}$$

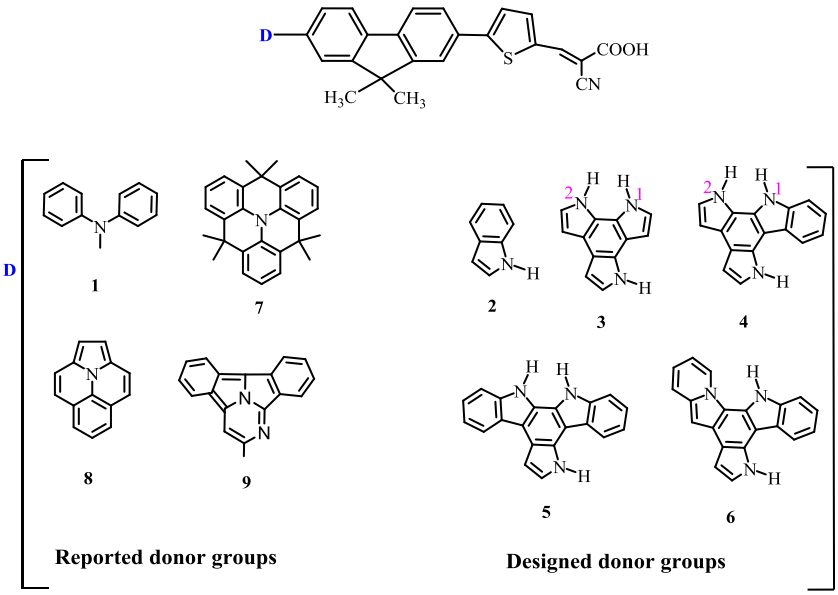

Fig. 1 Structures of organic dyes **1–9**

E^{dye*} can be expressed as [74]

$$E^{dye*} = E^{dye} - \lambda_{max}, \quad (4)$$

where E^{dye} is the redox potential of the ground state of the dye and λ_{max} is the vertical transition energy. The regeneration efficiency (η_{regen}) of the oxidized dye is associated with the regeneration driving force (ΔG_{regen}). ΔG_{regen} is the difference between the oxidation potential of the dye and the redox potential of the electrolyte I^-/I_3^- (4.58 eV) [75]. Thus, J_{sc} will increase with increasing LHE and ΔG_{inject}. The value of J_{sc} also increases when the value of ΔG_{regen} is decreased.

The V_{oc} of a DSSC is determined using the following equation [73]:

$$V_{oc} = \frac{E_c + \Delta CB}{q} + \frac{kT}{q}\ln\left(\frac{n_c}{N_{CB}}\right) - \frac{E_{redox}}{q}. \quad (5)$$

Here, q is a unit of charge, E_c is the conduction band edge of the semiconductor substrate, k is the Boltzmann constant, T is the absolute temperature, n_c is the number of electrons in the conduction band, N_{CB} is the density of accessible states in the conduction band, and E_{redox} is the reduction–oxidation potential of the electrolyte. ΔCB is the shift in the edge of the conduction band of the semiconductor when the dye is adsorbed at its surface [76].

Computational details

We applied DFT using Becke's three-parameter hybrid functional and the correlation formula of Lee, Yang, and Parr (B3LYP) [77, 78] for the gas-phase geometry optimization of compounds **1–9** before and after they were bound to the TiO_2 surface. The dyes were fully optimized using the 6-31G* basis set for the atoms C, H, O, N, and S and the effective core potential (ECP) basis set LANL2DZ for Ti atoms. Positive vibrational frequencies were obtained, confirming that the optimized molecular structures corresponded to energy minima. An earlier report had shown that this method could provide a reasonable prediction of the geometry—comparable to that optimized at the MP2 level of theory, but with a much lower computational cost [37]. The absorption spectra of the optimized dyes were obtained in the solvent tetrahydrofuran (THF) [79, 80] at the CPCM–CAM–B3LYP/6-31+G* [81] level of theory. The long-range corrected functional CAM-B3LYP showed the best agreement of λ_{max} with the experimentally observed results among all of the DFT functionals tested (Table S1 of the "Electronic supplementary material," ESM). We utilized the CAM-B3LYP functional in this study, as this method has been extensively employed to calculate the vertical transition energies of D–π–A dye molecules [38, 39, 82]. The oxidation potentials of the optimized free dyes were calculated at the CPCM-B3LYP/6-311G** level of theory for the neutral and the cationic dyes in the ground state [77]. Dipole moments of the TiO_2-bound dyes were calculated at the CPCM–B3LYP/6-31G* level of theory. $Ti(OH)_3H_2O$ was used as a model in earlier reports, and the results obtained with this model provided a reasonable explanation for the electronic and physical properties of TiO_2 [70]. This model also showed good agreement (in terms of electronic and physical properties) with a larger nanocluster, $(TiO_2)_6$ [83, 84]. All quantum chemical calculations carried out in the present work were performed using Gaussian 09 [85].

Results and discussion

Molecular design and geometries

The optimized geometries of the studied dyes **1–9** are shown in Fig. 2. The dye molecules anchored on the semiconductor TiO_2 model system are shown in Fig. S1 in the ESM. The basic unit of each dye molecule is D–π–A, where D is the donor group, which was always a cyclic asymmetric benzotripyrrole derivative. The phenyl-substituted derivative of cyclic asymmetric benzotripyrrole was prepared by the electropolymerization of indole-5-carboxylic acid and 5-cyanoindole [67]. The reaction of indole with nitrosobenzene in the presence of an acid also gives similar products [68]. Ruiz et al. ascertained that asymmetric compounds showed redshifted absorption and emission maxima compared to the maxima of the corresponding symmetric compounds [69]. Cyanoacrylic acid was used as an anchoring as well as an electron-acceptor group in dye molecules **2–6**. Fluorene and thiophene groups were attached between the chromophore and the anchoring group as π-spacer units. Such π-spacers are widely used in DSSCs to shift the absorption band into the visible region via extended π-conjugation [86]. Fluorene is a well-documented π-spacer that is used in organic dyes due to its photophysical and electrochemical properties [87]. This compound also influences DSSC efficiency due to its high molar extinction coefficient and light-harvesting properties [88–90]. Thiophene spacers have also been adopted for use in DSSCs due to their high polarizability, tunable spectroscopy, and electrochemical properties [91].

The effect of the choice of donor group on the geometrical structures of the designed dyes was examined (see Fig. 1 and Scheme 1). Some of the geometric parameters of the studied dyes (**1–9**) are listed in Table 1. The process of transferring an electron from the donor moiety to the semiconductor surface is facilitated (and thus solar cell efficiency can be increased) by D–π–A coplanarity. The calculated dihedral angles (θ) of **1–9** indicate that the constituent units in each of the dyes **2–6**

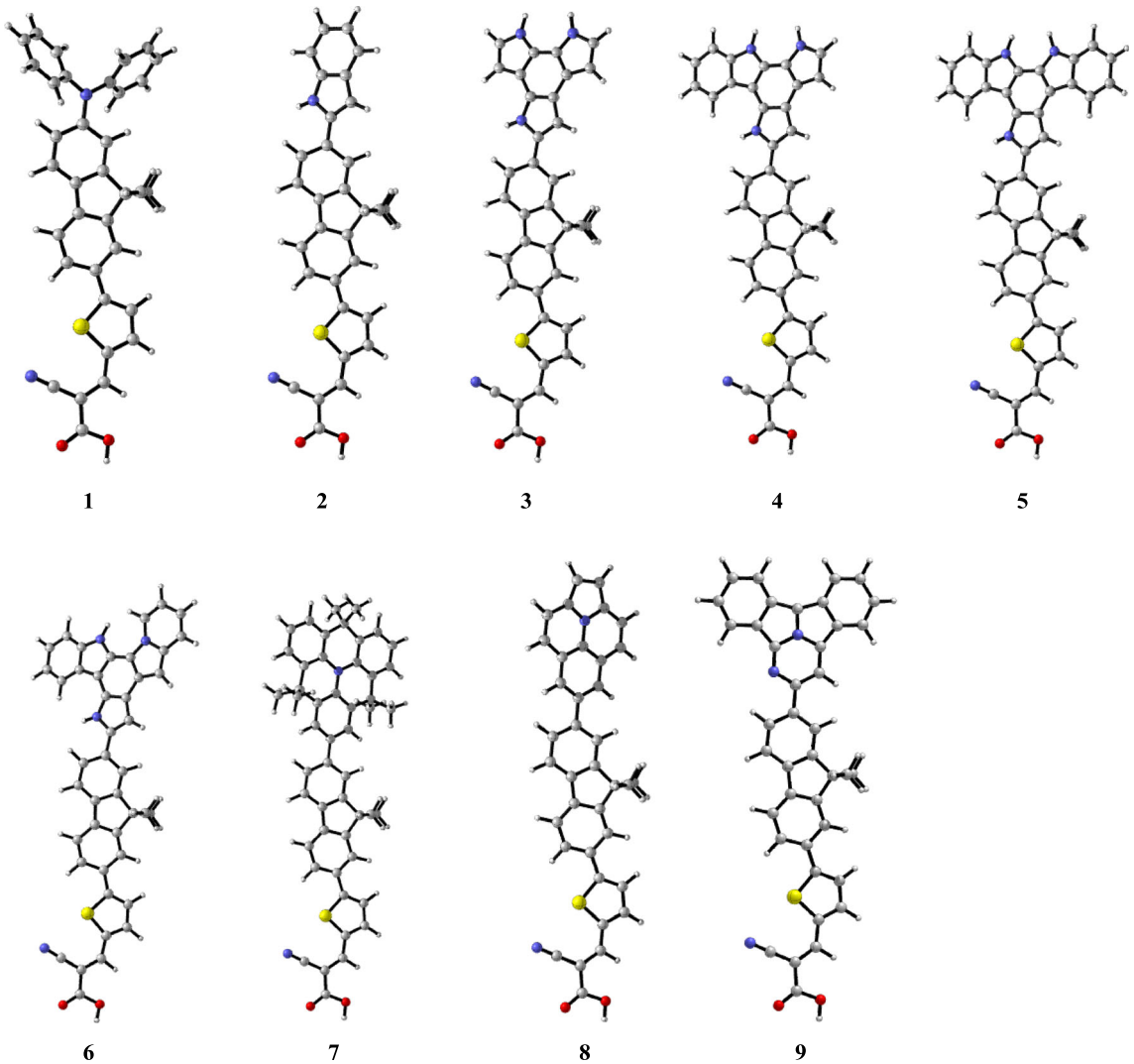

Fig. 2 Optimized geometries of the free dyes **1–9**, calculated at the B3LYP/6-31G* level of theory

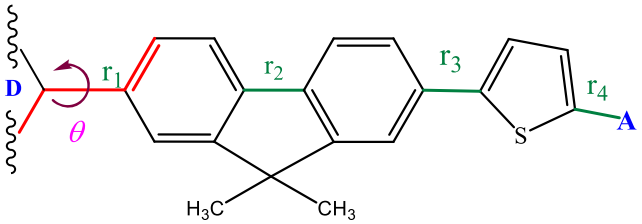

Scheme 1 D–π–A organic dyes: θ is the dihedral angle between the donor and spacer units (shown in *red*); r_1, r_2, r_3, and r_4 are bond lengths

and **9** are almost coplanar (Table 1 and Scheme 1). These dye molecules therefore show stronger π-conjugation effects than the other dye molecules studied here.

The frontier molecular orbitals of dyes **1–9** in the ground state are given in Fig. 3. Upon analyzing the frontier molecular orbitals, it was observed that the highest molecular orbital (HOMO) was mainly localized on the donor group and the fluorene spacer unit (Fig. 3) while the lowest unoccupied molecular orbital (LUMO) was mainly localized on the thiophene spacer and the acceptor group in the dye molecules (Fig. 3). The calculated energy levels of dyes **1–9**, along with the conduction band of the TiO_2 surface and the redox couple triiodide/iodide, are given in Fig. 4. Electron transfer from the dye molecule to the semiconductor occurs via two different mechanisms: type I or indirect injection and type II or direct injection [92, 93]. The type I process involves two steps: an excitation from the ground state to the excited state of the dye molecule that occurs through the absorption of a photon, and the transfer of an electron to the conduction band of the semiconductor nanoparticle (NP). The type II process involves a single step, in which the electron is transferred from the ground state of the dye to the conduction band of the semiconductor upon photoabsorption. It is known that, for the indirect mechanism to operate, the LUMO level must be above the conduction band of TiO_2 (E_{CB}, −4.00 eV) to allow effective electron injection, and the HOMO level should be lower than the redox potential of I^-/I_3^- (−4.80 eV) [73, 94]. The studied dyes utilize the indirect mechanism for electron transfer to the semiconductor nanoparticle (Fig. 4). It is clear from Fig. 4 that the HOMOs are situated below the redox potential of the I^-/I_3^- electrolyte (−4.80 eV), and that the LUMOs of all dyes lie above the conduction band of the TiO_2 surface [73, 94]. Thus, all of the designed dyes show favorable electron injection properties. Among the series of dye molecules, **6** has the lowest HOMO–LUMO energy gap (HLG), which facilitates electron excitation as well as longer-wavelength light absorption (Fig. 4).

Table 1 Selected bond lengths (r_1, r_2, r_3, and r_4, in Å), dihedral angles (θ, in degrees), and the HOMO–LUMO energy gaps (HLGs, in eV) of the designed dyes **1–9**

Dye	r_1	r_2	r_3	r_4	θ	HLG
1	1.416	1.461	1.462	1.425	−141.44	4.56
2	1.462	1.462	1.463	1.426	156.49	4.75
3	1.457	1.460	1.462	1.425	159.42	4.17
4	1.458	1.461	1.462	1.425	158.37	4.13
5	1.459	1.461	1.462	1.425	158.17	4.26
6	1.458	1.461	1.462	1.425	158.51	3.96
7	1.481	1.463	1.462	1.426	−143.07	4.29
8	1.486	1.463	1.463	1.426	−140.99	4.34
9	1.482	1.462	1.462	1.426	−160.27	4.30

Absorption spectra

The calculated maximum absorption wavelength (λ_{max}), the corresponding electronic transition configurations, the oscillator strengths (f), and the light-harvesting efficiencies (LHEs) of dyes **1–9** are listed in Table 2. The absorption spectrum of an organic dye is dependent on the conjugation present in the molecule, the dihedral angle between the donor and spacer groups, and the HOMO–LUMO energy gap for the probable transition. The degree of conjugation in the dye molecule influences the optical properties of the DSSC, and thus its efficiency [66, 71]. We also exploited the effect of π-conjugation at the appropriate position of the donor group to enhance DSSC efficiency. The calculated absorption spectrum of dye **2** was found to be 420 nm (Table 2). We attached two pyrrole groups to the phenyl ring of dye molecule **2** to create dye **3** (Fig. 1), enhancing the absorption wavelength. The absorption maximum of dye **3** was found to occur at 439 nm, suggesting increased conjugation in **3** than in **2** (Table 2, Fig. S3 in the ESM). The calculated dihedral angles for **2** and **3** corroborate the notion that the constituent units in **3** are more coplanar than those in **2** (Table 1). The calculated smaller HOMO–LUMO energy gap of dye **3** (4.17 eV) compared to that of dye **2** (4.77 eV) also shows the effect of the enhanced conjugation in the former case (Fig. 4, Table 1). One phenyl ring was then attached to the pyrrole unit of dye **3** to give dye **4** (Fig. 1). The calculated results revealed that dye **4** has a comparable absorption maximum (λ_{max} = 440 nm) to that of dye **3** (Table 2 and Fig. S3 in the ESM). Incorporation of a phenyl ring into dye **4** to yield dye **5**, however, shifted the absorption maximum to a lower wavelength (434 nm). Geometrical analysis of the optimized dye **5** suggested that the dihedral angle between the nitrogen atoms is larger ($N^1CCN^2 = -2.6°$) than in dye **4** ($N^1CCN^2 = -0.4°$) (Fig. 1). This distortion in the ring plane decreases the conjugation in dye **5** compared to dye **4**. This interrupted conjugation is reflected in the HOMO–LUMO energy gaps (HLGs) of the dyes. The HLG value of compound **5** (4.26 eV) is higher than that of **4** (4.13 eV) (Fig. 4, Table 1). To minimize the geometrical distortion in dye **5**, we changed the position of the phenyl ring attached to the pyrrole unit of dye **4** to generate dye **6** (Table 2). Dye **6**

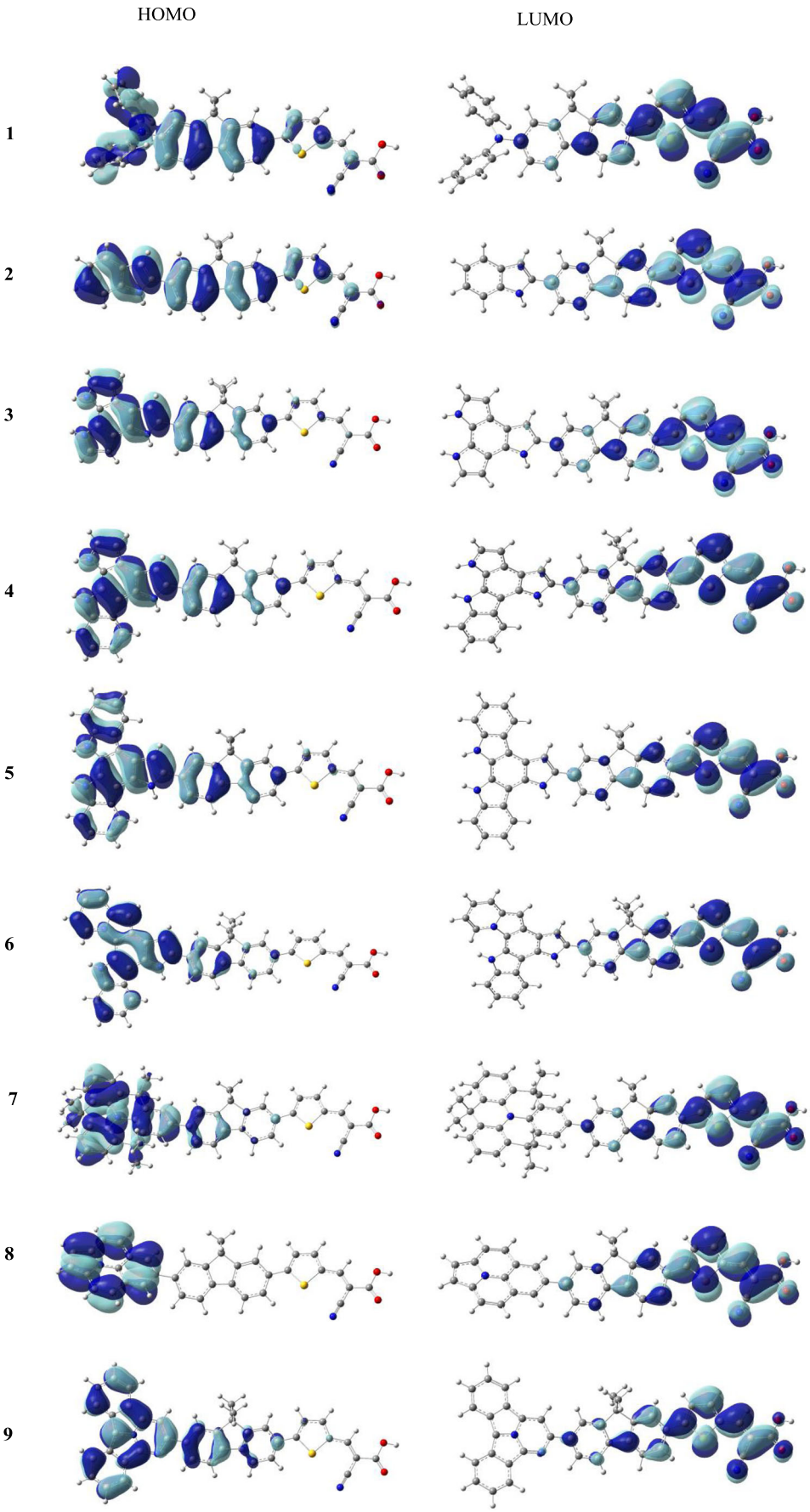

Fig. 3 HOMO–LUMO diagrams of dyes **1–9** calculated at the CAM–B3LYP/6-31 + G*// B3LYP/6-31G* level of theory in the gas phase; surfaces shown in the diagrams correspond to an isosurface value of 0.02

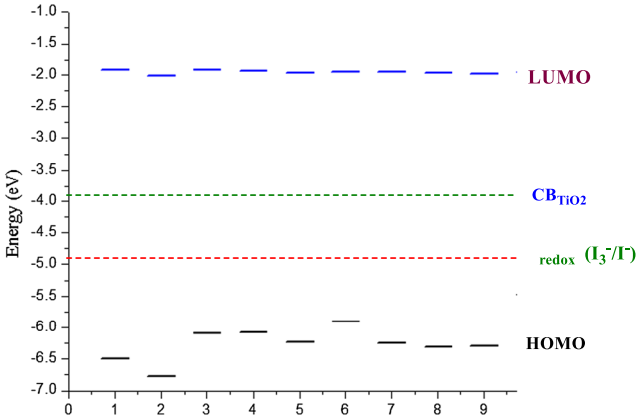

Fig. 4 Energy diagram showing the HOMO–LUMO gaps for dyes **1–9** (plotted along the *x*-axis), TiO_2, and the electrolyte (I_3^-/I^-)

showed a longer-wavelength absorption maximum (443 nm) due to better conjugation, which decreased the HOMO–LUMO gap. The computed absorption maxima of dyes **7–9** are also given in Table 2. The absorption maxima of dyes **7–9** occurred at smaller wavelengths than those of dye **6** and reference dye **1**.

Photovoltaic performance

Factors influencing J_{sc}

An important parameter of the dyes in relation to enhancing the efficiency of a DSSC is J_{sc}, which is directly related to the light-harvesting efficiency (LHE) and electron-injection rate (Φ_{inject}) of the dye (Eq. 2). The efficiency of a DSSC increases with increasing LHE and Φ_{inject} of the dye molecule. The calculated results for LHE, the electron-injection driving force (ΔG_{inject}), and the electron-regeneration driving force (ΔG_{regen}) are given in Table 3. The electron-injection driving force (ΔG_{inject}) can be calculated by relaxing or fixing the TiO_2 surface. An earlier study showed that a fixed surface of semiconducting TiO_2 yields reasonably close results to those observed experimentally [70]. Therefore, we assumed a fixed surface for calculations of the electron-injection driving force. The calculated LHE and oscillator strength values were found to increase with the degree of conjugation in the system (Table 2). The designed dyes (**2–6**) showed higher LHE values than reference dye **1** (0.98). Such LHE values are similar to some of the LHE values obtained for highly efficient organic dye molecules reported in the literature [95, 96]. These designed dye molecules (**2–6**) also show better LHE values than dye **10** (LHE = 0.98, η = 4.92 %), which is reported to be inferior to dye **1** (LHE = 0.99, η = 6.78 %) [70]. The ΔG_{inject} values of compounds **1–9** are given in Table 3. The calculated ΔG_{inject} value of reference compound **1** is −1.62 eV. It is known that ΔG_{inject} is related to J_{sc} and that the J_{sc} value of a dye increases with increasing ΔG_{inject}. The asymmetric benzotripyrrole donor dyes presented higher ΔG_{inject} values than that of **1** (Table 3). However, there is another factor, ΔG_{regen}, which also influences J_{sc} [97]. The larger the value of ΔG_{regen}, the lower the J_{sc} of a cell. We also calculated the ΔG_{regen} values for dyes **1–9**, as shown in Table 3. The calculated values suggest that dyes **3–6** have lower ΔG_{regen} values than dye **1**. Therefore, dyes **3–6** should have higher J_{sc} values than dye **1**. Furthermore, we compared the most promising dye, **6**, with other recently reported donor dye molecules (**7–9**) that have a donor nitrogen atom in the middle of the ring system. The computed results suggest that dye **6** should have a larger J_{sc} than dyes **7–9** due to the different positions of the nitrogen atoms in their ring systems; this difference leads to improved optical and electronic properties for **6**. The location of the nitrogen atom at a peripheral site in the ring in **6** significantly enhances λ_{max}, ΔG_{inject}, and ΔG_{regen} compared to the systems where the nitrogen is positioned in the middle of the ring (**7–9**). Therefore, it appears

Table 2 Calculated wavelengths of maximum absorption λ_{max} (in nm and in eV in parentheses), oscillator strengths *f*, light-harvesting efficiencies (LHEs), and the nature of the transitions for dyes **1–9**

Dye	State	λ_{max}	Main configuration	*f*	LHE
1	$S_0 \rightarrow S_1$	434 (2.86)	H-1 → L (0.32) H → L (0.59)	1.63	0.98
2	$S_0 \rightarrow S_1$	420 (2.96)	H-1 → L (0. 35) H → L (0.52)	1.85	0.99
3	$S_0 \rightarrow S_1$	439 (2.83)	H → L (0.49) H → L+1 (0.18)	1.93	0.99
4	$S_0 \rightarrow S_1$	440 (2.82)	H-2 → L (0.42) H → L (0.49)	1.96	0.99
5	$S_0 \rightarrow S_1$	434 (2.86)	H-2 → L (0.44) H → L (0.47)	2.06	0.99
6	$S_0 \rightarrow S_1$	443 (2.80)	H-2 → L (0.34) H → L (0. 46)	2. 01	0.99
7	$S_0 \rightarrow S_1$	420 (2.96)	H-1 → L (0. 56) H → L (-0.33)	1.85	0.99
8	$S_0 \rightarrow S_1$	414 (2.84)	H-1 → L (0. 59) H-2 → L (0.33)	1.78	0.98
9	$S_0 \rightarrow S_1$	428 (2.90)	H-1 → L (0. 48) H → L (0.41)	2.03	0.99

Table 3 Calculated values of the redox potential (E^{dye}, eV), driving force for electron injection (ΔG_{inject}, eV), and driving force for electron regeneration (ΔG_{regen}, eV) for dyes **1–9**

Dye	E^{dye}	ΔG_{inject}	ΔG_{regen}
1	5.24	−1.62	−0.66
2	5.59	−1.37	−1.01
3	5.02	−1.81	−0.47
4	4.99	−1.83	−0.41
5	5.10	−1.76	−0.52
6	4.85	−1.95	−0.27
7	5.10	−1.86	−0.52
8	5.24	−1.60	−0.66
9	5.24	−1.66	−0.66

Table 4 Computed atomic charge distributions (in units of *e*) on the donor, π-spacer, acceptor, and TiO_2 surface for dyes **1–9** adsorbed on the TiO_2 substrate in the ground state (S_0) and excited state (S_1), as calculated at the CPCM–B3LYP/6-31G* level

Dye	S_0					S_1				
	D	π	A	Ti[a]	μ_{normal}	D	π	A	Ti[a]	Δq
1	−0.119	0.327	−0.636	0.429	6.94	0.337	0.267	−0.949	0.346	0.083
2	0.026	0.176	−0.631	0.432	−4.38	0.456	0.125	−0.935	0.352	0.071
3	0.072	0.136	−0.637	0.429	12.19	0.730	0.011	−0.974	0.342	0.087
4	0.066	0.140	−0.636	0.431	12.02	0.739	−0.108	−0.974	0.342	0.089
5	0.051	0.152	−0.634	0.430	−10.02	0.714	−0.087	−0.971	0.345	0.085
6	0.144	−0.061	−0.635	0.430	10.36	0.822	−0.178	−0.985	0.338	0.092
7	0.017	0.183	−0.631	0.430	6.99	0.832	−0.173	−0.996	0.337	0.093
8	0.005	0.195	−0.628	0.427	6.21	0.932	−0.261	−1.006	0.337	0.090
9	−0.248	0.193	−0.631	0.432	6.97	0.694	−0.072	−0.971	0.345	0.087

[a] The TiO_2 substrate was modeled using $Ti(OH)_3H_2O$

that the efficiency of organic dye molecules can be tuned by varying the position of the donor nitrogen atom in the ring system.

Factors influencing V_{oc}

The overall power conversion efficiency of a solar cell also depends on the open-circuit photovoltage (V_{oc}) according to Eq. 1. It is known that the value of V_{oc} for a dye molecule can depend on the conduction band (CB), which is associated with the dipole moment of the molecule [98]. Grätzel and co-workers showed that the large vertical dipole moment (μ_{normal}) of an adsorbed dye molecule pointing away from the TiO_2 surface can significantly enhance V_{oc} and affect the efficiency of a dye-sensitized solar cell [99]. A $Ti(OH)_3H_2O$ model of the semiconductor surface was employed in a study and was found to adequately reproduce the properties of the semiconductor surface [70]. We expanded on this model of the TiO_2 surface by using a $(TiO_2)_6$ cluster model to examine the dipole moments, absorption spectra, and the main

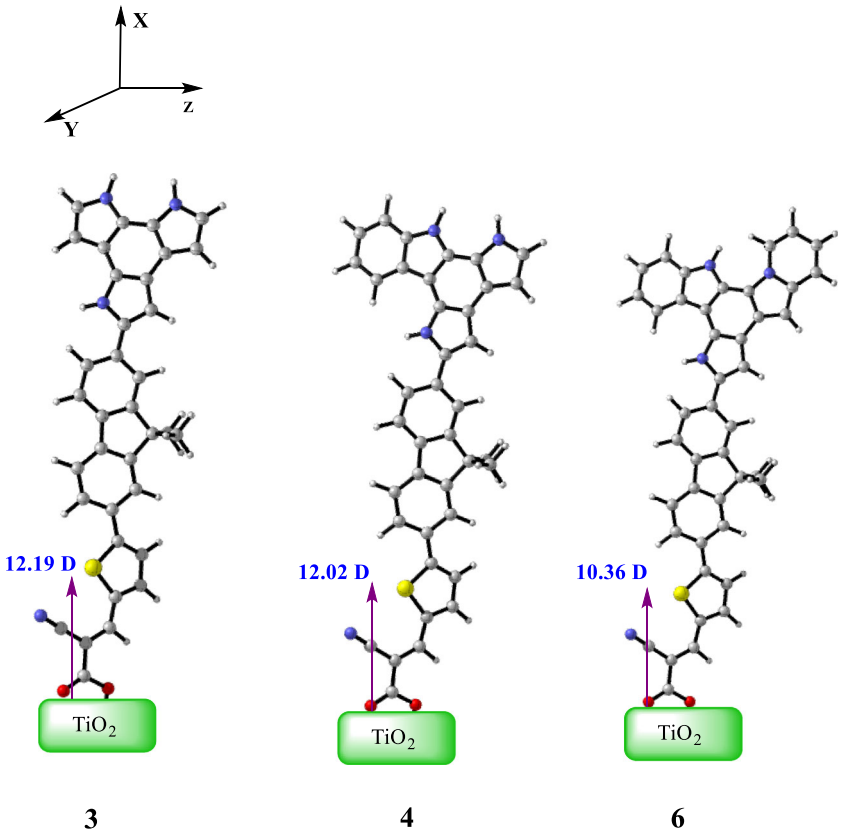

Fig. 5 Vertical dipole moments of dyes **3**, **4**, and **6**, as calculated at the CPCM–B3LYP/6-31G* level of theory. The TiO_2 surface was considered to be parallel to the *yz*-plane

configurations of the spectra for dyes **4** and **6** as representative cases (Fig. S4, Tables S2–S4). The calculated results revealed that the trends afforded by the $(TiO_2)_6$ cluster model were similar to those obtained with the simpler $Ti(OH)_3H_2O$ model. The following equation can be used to calculate the shift in E_c for the semiconductor upon the adsorption of a dye molecule:

$$\Delta CB = -\frac{q\mu_{normal}\gamma}{\varepsilon_0\varepsilon}, \quad (6)$$

where μ_{normal} is the dipole moment of an individual dye molecule perpendicular to the surface of the semiconductor substrate, γ is the surface concentration of the dye, and ε_0 and ε represent the vacuum permittivity and the dielectric permittivity, respectively. It is evident from Eqs. 5 and 6 that increasing the μ_{normal} and n_c values of a dye will enhance the V_{oc}. Table 4 presents the values of n_c obtained by calculating the difference in the charge on the TiO_2 surface between the ground state (S_0) and excited state (S_1) for dyes **1–9**. We also calculated the μ_{normal} values for the studied dyes (Table 4 and Fig. 5). The calculated μ_{normal} and n_c values suggest that dyes **3**, **4**, and **6** should have much higher V_{oc} values than reference dye **1**. The dyes with donor units (**7–9**) that have a nitrogen in the middle of the ring showed lower μ_{normal} and n_c values than dye **6**.

Conclusions

In this work, we investigated a series of metal-free organic dyes (**2–6**) theoretically, and showed that their application in DSSCs should lead to improved efficiency. Cyclic asymmetric benzotripyrrole derivatives were modeled as the donor groups in these dye systems. The phenyl derivative of cyclic asymmetric benzotripyrroles can be obtained synthetically in the laboratory [67]. The results of our calculations indicate that dye **2** has lower efficiency than reference dye **1**. The role of conjugation was examined, and the cyclic asymmetric benzotripyrrole unit was found to yield higher DSSC efficiency. Dyes **3** and **4** were predicted to have superior LHEs, ΔG_{inject} values, vertical dipole moments, and electron injection compared to reference dye **1**. The V_{oc} values of dyes **3** and **4** were enhanced because of an improved electron-transfer process and higher vertical dipole moments compared to dye **1**. Dyes **3** and **4** also showed higher J_{sc} values than dye **1**. The designed dye **6** presented the highest λ_{max} (443 nm) among the studied series of dye molecules due to its increased conjugation, which influences the HUMO–LUMO energy gap. The calculated LHE, ΔG_{inject}, μ_{normal}, and Δq values suggest that dye **6** should permit the largest improvement in DSSC efficiency among the series of dye molecules **1–6**. We also compared the photophysical properties of dye **6** with those of other reported dyes **7–9** that have a donor nitrogen atom is in the middle of the ring system. The computed results predicted that designed dye **6** should possess a higher incident photon to current conversion efficiency (IPCE) than the reported dyes **7–9**. The locations of the nitrogen atoms in the donor groups in the designed dye molecules were found to be an important influence on DSSC efficiency, with peripheral locations of the nitrogen atoms leading to enhanced efficiency. Such results may contribute towards the development of more efficient dyes for solar cell applications.

Acknowledgments The authors thank MSM (CSIR, New Delhi) as well as SIP and CSIR (New Delhi) for financially supporting this work. AKB is grateful to UGC (New Delhi) for awarding the senior research fellowship and to AcSIR for Ph.D. enrollment. The authors also gratefully acknowledge the computer resources provided by CSIR-NCL, Pune (India). This report is CSIR-CSMCRI communication number 147/2014. Finally, we thank the reviewer for providing valuable suggestions/comments that helped us to improve the paper.

Compliance with ethical standards

Conflict of Interest The authors declare that they have no conflict of interest.

References

1. Hagfeldt A, Boschloo G, Sun L, Kloo L, Pettersson H (2010) Dye sensitized solar cells. Chem Rev 110:6595–663
2. Liang M, Chen J (2013) Arylamine organic dyes for dye-sensitized solar cells. Chem Soc Rev 42:3453–3488
3. Maggio E, Solomon GC, Troisi A (2014) Exploiting quantum interference in dye sensitized solar cells. ACS Nano 8:409–418
4. Brédas JL, Norton JE, Cornil J, Coropceanu V (2009) Molecular understanding of organic solar cells: the challenges. Acc Chem Res 42:1691–1699
5. Yang J, Ganesan P, Teuscher J, Moehl T, Kim YJ, Yi C, Comte P, Pei K, Holcombe TW, Nazeeruddin MK, Hua J, Zakeeruddin SM, Tian H, Grätzel M (2014) Influence of the donor size in D–π–A organic dyes for dye-sensitized solar cells. J Am Chem Soc 136:5722–5730
6. Nguyen WH, Bailie CD, Unger Eva L, McGehee MD (2014) Enhancing the hole-conductivity of spiro-OMeTAD without oxygen or lithium salts by using spiro $(TFSI)_2$ in perovskite and dye-sensitized solar cells. J Am Chem Soc 136:10996–11001
7. Kang X, Zhang J, O'Neil D, Rojas AJ, Chen W, Szymanski P, Marder SR, El-Sayed MA (2014) Effect of molecular structure perturbations on the performance of the D–A–π–A dye sensitized solar cells. Chem Mater 26:4486–4493
8. Stalder R, Xie D, Islam A, Han L, Reynolds JR, Schanze KS (2014) Panchromatic donor–acceptor–donor conjugated oligomers for dye-sensitized solar cell applications. ACS Appl Mater Interfaces 6:8715–8722
9. Yella A, Lee HW, Tsao HN, Yi C, Chandiran AK, Nazeeruddin MK, Diau EWG, Yeh CY, Zakeeruddin SM, Grätzel M (2011) Porphyrin-sensitized solar sells with cobalt(II/III)-based redox electrolyte exceed 12% efficiency. Science 334:629–634
10. O'Regan B, Grätzel M (1991) A low-cost, high-efficiency solar cell based on dye-sensitized colloidal TiO_2 films. Nature 353:737–740
11. Ushiroda S, Ruzycki N, Lu Y, Spitler MT, Parkinson BA (2005) Dye sensitization of the anatase (101) crystal surface by a series of dicarboxylated thiacyanine dyes. J Am Chem Soc 127:5158–5168

12. Mathew S, Yella A, Gao P, Humphry-Baker R, Curchod BFE, Ashari-Astani N, Tavernelli I, Rothlisberger U, Nazeeruddin MK, Grätzel M (2014) Dye-sensitized solar cells with 13% efficiency achieved through the molecular engineering of porphyrin sensitizers. Nat Chem 6:242–247
13. Li LL, Diau EWG (2012) Porphyrin-sensitized solar cells. Chem Soc Rev 42:291–304
14. Chou CC, Hu FC, Wu KL, Duan T, Chi Y, Liu SH, Lee GH, Chou PT (2014) 4,4′,5,5′-Tetracarboxy-2,2′-bipyridine Ru(II) sensitizers for dye-sensitized solar cells. Inorg Chem 53:8593–8599
15. Luo J, Xu M, Li R, Huang KW, Jiang C, Qi Q, Zeng W, Zhang J, Chi C, Wang P, Wu J (2014) N-annulated perylene as an efficient electron donor for porphyrin-based dyes: enhanced light-harvesting ability and high-efficiency Co(II/III)-based dye-sensitized solar cells. J Am Chem Soc 136:265–272
16. Wang SW, Wu KL, Ghadiri E, Lobello MG, Ho ST, Chi Y, Moser J, Angelis FD, Grätzel M, Nazeeruddin MK (2013) Engineering of thiocyanate-free Ru(II) sensitizers for high efficiency dye-sensitized solar cells. Chem Sci 4:2423–2433
17. Sinn S, Schulze B, Friebe C, Brown DG, Jäger M, Kübel J, Dietzek B, Berlinguette CP, Schubert US (2014) A heteroleptic bis(tridentate) ruthenium(II) platform featuring an anionic 1,2,3-triazolate-based ligand for application in the dye-sensitized solar cell. Inorg Chem 53:1637–1645
18. Wang P, Klein C, Humphry-Baker R, Zakeeruddin SM, Grätzel M (2005) A high molar extinction coefficient sensitizer for stable dye-sensitized solar cells. J Am Chem Soc 127:808–809
19. Swierk JR, McCool NS, Saunders TP, Barber GD, Mallouk TE (2014) Effects of electron trapping and protonation on the efficiency of water-splitting dye-sensitized solar cells. J Am Chem Soc 136:10974–10982
20. El-Shafeil A, Hussain M, Islam A, Han L (2014) Structure–property relationship of hetero-aromatic-electron-donor antennas of polypyridyl Ru(II) complexes for high efficiency dye-sensitized solar cells. Prog Photovolt Res Appl 22:958–969
21. Cheema H, Islam A, Han L, El-Shafei A (2014) Influence of number of benzodioxan-stilbazole-based ancillary ligands on dye packing, photovoltage and photocurrent in dye-sensitized solar cells. ACS Appl Mater Interfaces 6:11617–11624
22. Nazeeruddin MK, Pechy P, Renouard T, Zakeeruddin SM, Humphry-Baker R, Comte P, Liska P, Cevey L, Costa E, Shklover V, Spiccia L, Deacon GB, Bignozzi CA, Grätzel M (2001) Engineering of efficient panchromatic sensitizers for nanocrystalline TiO_2-based solar cells. J Am Chem Soc 123:1613–1624
23. Selopal GS, Memarian N, Milan R, Concina I, Sberveglieri G, Vomiero A (2014) Effect of blocking layer to boost photoconversion efficiency in ZnO dye-sensitized solar cells. ACS Appl Mater Interfaces 6:11236–11244
24. Ozawa H, Sugiura T, Shimizu R, Arakawa H (2014) Novel ruthenium sensitizers having different numbers of carboxyl groups for dye-sensitized solar cells: effects of the adsorption manner at the TiO_2 surface on the solar cell performance. Inorg Chem 53: 9375–9384
25. Bomben PG, Gordon TJ, Schott E, Berlinguette CP (2011) A trisheteroleptic cyclometalated Ru^{II} sensitizer that enables high power output in a dye-sensitized solar cell. Angew Chem Int Ed 50:10682–10685
26. Mishra A, Fischer MKR, Bäuerle P (2009) Metal-free organic dyes for dye-sensitized solar cells: from structure: property relationships to design rules. Angew Chem Int Ed 48: 2474–2499
27. Hara K, Sato T, Katoh R, Furube A, Yoshihara T, Murai M, Kurashige M, Ito S, Shinpo A, Suga S, Arakawa H (2005) Novel conjugated organic dyes for efficient dye-sensitized solar cells. Adv Funct Mater 15:246–252
28. Teng C, Yang X, Yang C, Li S, Cheng M, Hagfeldt A, Sun L (2010) Molecular design of anthracene-bridged metal-free organic dyes for efficient dye-sensitized solar cells. J Phys Chem C 114:9101–9110
29. Ito S, Zakeeruddin SM, Humphry-Baker R, Liska P, Charvet R, Comte P, Nazeeruddin MK, Péchy P, Takata M, Miura H, Uchida S, Grätzel M (2006) High-efficiency organic-dye-sensitized solar cells controlled by nanocrystalline–TiO_2 electrode thickness. Adv Mater 18:1202–1205
30. Hwang S, Lee JH, Park C, Lee H, Kim C, Park C, Lee MH, Lee W, Park J, Kim K, Park NG, Kim C (2007) A highly efficient organic sensitizer for dye-sensitized solar cells. Chem Commun 4887–4889
31. Ito S, Miura H, Uchida S, Takata M, Sumioka K, Liska P, Comte P, Pechy P, Grätzel M (2008) High-conversion-efficiency organic dye-sensitized solar cells with a novel indoline dye. Chem Commun 5194–5196
32. Abbotto A, Manfredi N, Marinzi C, Angelis FD, Mosconi E, Yum JH, Xanxi Z, Nazeeruddin MK, Grätzel M (2009) Di-branched di-anchoring organic dyes for dye-sensitized solar cells. Energy Environ Sci 2:1094–1101
33. Ambrosio F, Martsinovich N, Troisi A (2012) What is the best anchoring group for a dye in a dye-sensitized solar cell? J Phys Chem Lett 3:1531–1535
34. Chen CH, Hsu YC, Chou HH, Thomas KRJ, Lin JT, Hsu CP (2010) Dipolar compounds containing fluorene and a heteroaromatic ring as the conjugating bridge for high-performance dye-sensitized solar cells. Chem Eur J 16:3184–3193
35. Zoppi L, Martin-Samos L, Baldridge KK (2014) Structure–property relationships of curved aromatic materials from first principles. Acc Chem Res 47:3310–3320
36. Jacquemin D, Wathelet V, Perpete EA, Adamo C (2009) Extensive TD-DFT benchmark: singlet-excited states of organic molecules. J Chem Theory Comput 5:2420–2435
37. Preat J, Michaux C, Jacquemin D, Perpète EA (2009) Enhanced efficiency of organic dye-sensitized solar cells: triphenylamine derivatives. J Phys Chem C 113:16821–16833
38. Preat J, Jacquemin D, Michaux C, Perpète EA (2010) Improvement of the efficiency of thiophene-bridged compounds for dye-sensitized solar cells. Chem Phys 376:56–58
39. Preat J (2010) Photoinduced energy-transfer and electron-transfer processes in dye-sensitized solar cells: TDDFT insights for triphenylamine dyes. J Phys Chem C 114:16716–16725
40. Martsinovich N, Troisi A (2011) High-throughput computational screening of chromophores for dye-sensitized solar cells. J Phys Chem C 115:11781–11792
41. de Sanchez Armas R, San-Miguel MA, Oviedo J, Sanz JF (2012) Molecular modification of coumarin dyes for more efficient dye sensitized solar cells. J Chem Phys 136:194702–194707
42. Calbo J, Pastore M, Mosconi E, Ortí E, Angelis FD (2014) Computational modeling of single- versus double-anchoring modes in di-branched organic sensitizers on TiO_2 surfaces: structural and electronic properties. Phys Chem Chem Phys 16:4709–4719
43. Labat F, Bahers T, Ciofini I, Adamo C (2012) First-principles modeling of dye-sensitized solar cells: challenges and perspective. Acc Chem Res 45:1268–1277
44. McNamara WR, Snoeberger RC III, Li G, Schleicher JM, Cady CW, Poyatos M, Schmuttenmaer CA, Crabtree RH, Brudvig GW, Batista VS (2008) Acetylacetonate anchors for robust functionization of TiO_2 nanoparticles with Mn(II)–terpyridine complexes. J Am Chem Soc 130:14329–14338
45. Gu X, Zhou L, Li Y, Sun Q, Jena P (2012) Design of new metal-free dyes for dye sensitized solar cells: a first-principles study. Phys Lett A 376:2595–2599
46. Hara K, Kurashige M, Ito S, Shinpo A, Suga S, Sayama K, Arakawa H (2003) Novel polyene dyes for highly efficient dye-sensitized solar cells. Chem Commun 252–253

47. Wu G, Kong F, Zhang Y, Zhang X, Li J, Chen W, Liu W, Ding Y, Zhang C, Zhang B, Yao J, Dai S (2014) Multiple-anchoring triphenylamine dyes for dye-sensitized solar cell application. J Phys Chem C 118:8756–8765
48. Wang ZS, Cui Y, Dan-oh Y, Kasada C, Shinpo A, Hara K (2008) Molecular design of coumarin dyes for stable and efficient organic dye-sensitized solar cells. J Phys Chem C 112:17011–17017
49. Wang ZS, Cui Y, Dan-oh Y, Kasada C, Shinpo A, Hara K (2007) Thiophene-functionalized coumarin dye for efficient dye-sensitized solar cells: electron lifetime improved by coadsorption of deoxycholic acid. J Phys Chem C 111:7224–7230
50. Morandeira A, Boschloo G, Hagfeldt A, Hammarström L (2008) Coumarin 343–NiO films as nanostructured photocathodes in dye-sensitized solar cells: ultrafast electron transfer, effect of the I^{3-}/I^{-} redox couple and mechanism of photocurrent generation. J Phys Chem C 112:9530–9537
51. Hara K, Wang ZS, Sato T, Furube A, Katoh R, Sugihara H, Dan-oh Y, Kasada C, Shinpo A, Suga S (2005) Oligothiophene-containing coumarin dyes for efficient dye-sensitized solar cells. J Phys Chem B 109:15476–15482
52. Thongkasee P, Thangthong A, Janthasing N, Sudyoadsuk T, Namuangruk S, Keawin T, Jungsuttiwong S, Promarak V (2014) Carbazole-dendrimer-based donor–π–acceptor type organic dyes for dye-sensitized solar cells: effect of the size of the carbazole dendritic donor. ACS Appl Mater Interfaces 6:8212–8222
53. Uemura Y, Murakami TN, Koumura N (2014) Crown ether-substituted carbazole dye for dye-sensitized solar cells: controlling the local ion concentration at the TiO_2/dye/electrolyte interface. J Phys Chem C 118:16749–16759
54. Pei K, Wu Y, Islam A, Zhu S, Han L, Geng Z, Zhu W (2014) Dye-sensitized solar cells based on quinoxaline dyes: effect of π-linker on absorption, energy levels, and photovoltaic performances. J Phys Chem C 118:16552–16561
55. Lu X, Feng Q, Lan T, Zhou G, Wang ZS (2012) Molecular engineering of quinoxaline-based organic sensitizers for highly efficient and stable dye-sensitized solar cells. Chem Mater 24:3179–3187
56. Kim S, Lee JK, Kang SO, Ko J, Yum JH, Fantacci S, DeAngelis F, DiCenso D, Nazeeruddin MK, Grätzel M (2006) Molecular engineering of organic sensitizers for solar cell applications. J Am Chem Soc 128:16701–16707
57. Kim S, Choi H, Kim D, Song K, Kang SO, Ko J (2007) Novel conjugated organic dyes containing bis-dimethylfluorenyl amino phenyl thiophene for efficient solar cell. Tetrahedron 63:9206–9212
58. Kim S, Choi H, Baik C, Song K, Kang SO, Ko J (2007) Synthesis of conjugated organic dyes containing alkyl substituted thiophene for solar cell. Tetrahedron 63:11436–11443
59. Choi H, Baik C, Kang SO, Ko J, Kang MS, Nazeeruddin MK, Grätzel M (2008) Highly efficient and thermally stable organic sensitizers for solvent-free dye-sensitized solar cells. Angew Chem Int Ed 47:327–330
60. Jung I, Lee JK, Song KH, Song K, Kang SO, Ko J (2007) Synthesis and photovoltaic properties of efficient organic dyes containing the benzo[b]furan moiety for solar cells. J Org Chem 72:3652–3658
61. Kim D, Lee JK, Kang SO, Ko J (2007) Molecular engineering of organic dyes containing n-aryl carbazole moiety for solar cell. Tetrahedron 63:1913–1922
62. Choi H, Lee JK, Song KH, Song K, Kang SO, Ko J (2007) Synthesis of new julolidine dyes having bithiophene derivatives for solar cell. Tetrahedron 63:1553–1559
63. Choi H, Lee JK, Song K, Kang SO, Ko J (2007) Novel organic dyes containing bis-dimethylfluorenyl amino benzo[b]thiophene for highly efficient dye-sensitized solar cell. Tetrahedron 63: 3115–3121
64. Hagberg DP, Yum JH, Lee H, De Angelis F, Marinado T, Karlsson KM, Humphry-Baker R, Sun L, Hagfeldt A, Grätzel M, Nazeeruddin MK (2008) Molecular engineering of organic sensitizers for dye-sensitized solar cell applications. J Am Chem Soc 130:6259–6266
65. Li G, Jiang KJ, Li YF, Li SL, Yang LM (2008) Efficient structural modification of triphenylamine-based organic dyes for dye-sensitized solar cells. J Phys Chem C 112:11591–11599
66. Delcamp JH, Yella A, Holcombe TW, Nazeeruddin MK, Grätzel M (2013) The molecular engineering of organic sensitizers for solar-cell applications. Angew Chem Int Ed 52:376–380
67. Jennings P, Jones AC, Mountand AR, Thomson AD (1997) Electrooxidation of 5-substituted indoles. J Chem Soc Faraday Trans 93:3791–3797
68. Greci L, Tommasi G, Petrucci R, Marrosu G, Trazza A, Sgarabotto P, Righi L, Alberti A (2000) Oxidative trimerization of indole: on the formation of dications and radicalcations by reaction of indole and nitrosobenzene in the presence of acids. J Chem Soc Perkin Trans 2:2337–2342
69. Ruiz C, García-Frutos EM, Filho DADS, Navarrete JTL, Delgado MCR, Gómez-Lor B (2014) Symmetry lowering in triindoles: impact on the electronic and photophysical properties. J Phys Chem C 118:5470–5477
70. Ji Z, Li HB, Sun SL, Geng Y, Wu Y, Su ZM (2012) Density functional theory characterization and design of high-performance diarylamine-fluorene dyes with different π spacers for dye-sensitized solar cells. J Mater Chem 22:568–576
71. Biswas AK, Barik S, Sen A, Das A, Ganguly B (2014) Design of efficient metal-free organic dyes having an azacyclazine scaffold as the donor fragment for dye-sensitized solar cells. J Phys Chem C 118:20763–20771
72. Do K, Kim D, Cho N, Paek S, Song K, Ko J (2012) New type of organic sensitizers with a planar amine unit for efficient dye-sensitized solar cells. Org Lett 14:222–225
73. Katoh R, Furube A, Yoshihara T, Hara K, Fujihashi G, Takano S, Murata S, Arakawa H, Tachiya M (2004) Efficiencies of electron injection from excited N3 dye into nanocrystalline semiconductor (ZrO_2, TiO_2, ZnO, Nb_2O_5, SnO_2, In_2O_3) films. J Phys Chem C 108: 4818–4822
74. Marinado T, Nonomura K, Nissfolk J, Karlsson MK, Hagberg DP, Sun L, Mori S, Hagfeldt A (2009) How the nature of triphenylamine–polyene dyes in dye-sensitized solar cells affects the open-circuit voltage and electron lifetimes. Langmuir 26: 2592–2598
75. Bai Y, Zhang J, Zhou D, Wang Y, Zhang M, Wang P (2011) Engineering organic sensitizers for iodine-free dye-sensitized solar cells: red-shifted current response concomitant with attenuated charge recombination. J Am Chem Soc 133:11442–11445
76. Rühle S, Greenshtein M, Chen SG, Merson A, Pizem H, Sukenik CS, Cahen D, Zaban A (2005) Molecular adjustment of the electronic properties of nanoporous electrodes in dye-sensitized solar cells. J Phys Chem B 109:18907–18913
77. Becke AD (1993) Density-functional thermochemistry. III. The role of exact exchange. J Chem Phys 98:5648–5653
78. Lee C, Yang W, Parr RG (1988) Development of the Colle–Salvetti correlation–energy formula into a functional of the electron density. Phys Rev B 37:785–789
79. Karthikeyan S, Lee JY (2013) Zinc-porphyrin based dyes for dye-sensitized solar cells. J Phys Chem A 117:10973–10979
80. Balanay MP, Kim DH (2008) DFT/TD-DFT molecular design of porphyrin analogues for use in dye-sensitized solar cells. Phys Chem Chem Phys 10:5121–5127
81. Barone V, Cossi M (1998) Quantum calculation of molecular energies and energy gradients in solution by a conductor solvent model. J Phys Chem A 102:1995–2001
82. Pastore M, Mosconi E, De Angelis F, Grätzel M (2010) A computational investigation of organic dyes for dye-sensitized solar cells: benchmark, strategies, and open issues. J Phys Chem C 114: 7205–7212

83. Sánchez-de-Armas RO, Oviedo López J, San-Miguel MA, Sanz JF, Ordejón P, Pruneda M (2010) Real-time TD-DFT simulations in dye sensitized solar cells: the electronic absorption spectrum of alizarin supported on TiO_2 nanoclusters. J Chem Theory Comput 6:2856–2865
84. Sánchez-de-Armas RO, San-Miguel MA, Oviedo López J, Marquez A, Sanz JF (2011) Electronic structure and optical spectra of catechol on TiO_2 nanoparticles from real time TD-DFT simulations. Phys Chem Chem Phys 13:1506–1514
85. Frisch MJ, Trucks GW, Schlegel HB, Scuseria GE, Robb MA, Cheeseman JR, Scalmani G, Barone V, Mennucci B, Petersson GA et al (2013) Gaussian 09, revision D.01. Gaussian, Inc., Wallingford
86. Tian H, Yang X, Chen R, Zhang R, Hagfeldt A, Sun L (2008) Effect of different dye baths and dye-structures on the performance of dye-sensitized solar cells based on triphenylamine dyes. J Phys Chem C 112:11023–11033
87. Peng Z, Tao S, Zhang X, Tang J, Lee CS, Lee ST (2008) New fluorene derivatives for blue electroluminescent devices: influence of substituents on thermal properties, photoluminescence, and electroluminescence. J Phys Chem C 112:2165–2169
88. Baheti A, Singh P, Lee CP, Thomas KRJ, Ho KC (2011) 2,7-Diaminofluorene-based organic dyes for dye-sensitized solar cells: effect of auxiliary donor on optical and electrochemical properties. J Org Chem 76:4910–4920
89. Khan MS, Al-Mandhary MRA, Al-Suti MK, Ahrens B, Mahon MF, Male L, Raithby PR, Boothby CE, Kohler A (2003) Synthesis, characterisation and optical spectroscopy of diynes and poly-ynes containing derivatised fluorenes in the backbone. Dalton Trans 74–84
90. Wielopolski M, Santos J, Illescas BM, Ortiz A, Insuasty B, Bauer T, Clark T, Guldi DM, Martin N (2011) Vinyl spacers—tuning electron transfer through fluorene-based molecular wires. Energy Environ Sci 4:765–771
91. Chang DW, Tsao HN, Salvatori P, Angelis FD, Grätzel M, Park SM, Dai L, Lee HJ, Baek JB, Nazeeruddin MK (2012) Bistriphenylamine-based organic sensitizers with high molar extinction coefficients for dye-sensitized solar cells. RSC Adv 2: 6209–6215
92. Sánchez-de-Armas R, Oviedo J, Miguel MÁS, Sanz JF (2011) Direct vs indirect mechanisms for electron injection in dye-sensitized solar cells. J Phys Chem C 115:11293–11301
93. Oviedo MB, Zarate X, Negre CFA, Schott E, Arratia-Perez R, Sánchez CG (2012) Quantum dynamical simulations as a tool for predicting photoinjection mechanisms in dye-sensitized TiO_2 solar cells. J Phys Chem Lett 3:2548–2555
94. Zhang G, Bala H, Cheng Y, Shi D, Lv X, Yu Q, Wang P (2009) High efficiency and stable dye-sensitized solar cells with an organic chromophore featuring a binary π-conjugated spacer. Chem Commun 2198–2200
95. Feng J, Jiao Y, Ma W, Nazeeruddin MK, Grätzel M, Sheng M (2013) First principles design of dye molecules with ullazine donor for dye sensitized solar cells. J Phys Chem C 117:3772–3778
96. Zhang T, Guan W, Wen S, Ma T, Yan L, Su Z (2014) Theoretical studies on metalloporphyrin–polyoxometalates hybrid complexes for dye-sensitized solar cells. J Phys Chem C 118:29623–29628
97. Zhang J, Kan YH, Li HB, Geng Y, Wu Y, Su ZM (2012) How to design proper π-spacer order of the D–π–A dyes for DSSCs? A density functional response. Dyes Pigments 95:313–321
98. Ruhle S, Greenshtein M, Chen SG, Merson A, Pizem H, Sukenik CS, Cahen D, Zaban A (2005) Molecular adjustment of the electronic properties of nanoporous electrodes in dye-sensitized solar cells. J Phys Chem B 109:18907–18913
99. Chen P, Yum JH, Angelis FD, Mosconi E, Fantacci S, Moon SJ, Baker RH, Ko J, Nazeeruddin MK, Grätzel M (2009) High open-circuit voltage solid-state dye-sensitized solar cells with organic dye. Nano Lett 9:2487–2492